Journal of Power Sources 232 (2013) 199–208

Contents lists available at SciVerse ScienceDirect

Journal of Power Sources

journal homepage: www.elsevier.com/locate/jpowsour

Influences of operational factors on proton exchange membrane fuel cell performance with modified interdigitated flow field design

Hui-Wen Ku, Horng-Wen Wu*

Department of System and Naval Mechatronic Engineering, National Cheng Kung University, 1 Ta-Hsueh Road, Tainan 701, Taiwan, ROC

HIGHLIGHTS

- ► Using 3D model and Taguchi method in interdigitated channel gets optimal performance.
- ► Adding rectangular parallelepipeds increases the electrochemical reaction.
- ► Novel design generates more uniform current density and concentration distribution.
- ► The rectangular parallelepiped number over 8 has little enhancement for net power.
- ► The net power of the novel design 26% more than that of the original one.

ARTICLE INFO

Article history:
Received 21 August 2012
Received in revised form
2 January 2013
Accepted 3 January 2013
Available online 12 January 2013

Keywords:
Proton exchange membrane fuel cell
Rectangular parallelepipeds
Taguchi method
The interdigitated flow field

ABSTRACT

This paper presents a novel design of the rectangular parallelepiped within the interdigitated flow field to augment the performance of a PEM fuel cell by simulation and experiment. The numerical results indicate that the performance is enhanced with increasing the rectangular parallelepiped number because of stronger obstructing reactant gases through the channel to enter catalyst layers. In addition, the novel design is numerically obtained for the interdigitated flow field. The operational parameters are then determined by the Taguchi method on the experiment according to the novel design. The net power obtained is 26% greater for the novel design at the optimum parameter combination of $A_2B_3C_2D_2E_2$ than for the smooth-walled channel at the $A_2B_2C_2D_3E_3$.

1. Introduction

A proton exchange membrane (PEM) fuel cell has most drawn attention through its simplicity, viability, quick start-up, and pollution-free from reaction to form H_2O. In addition, it is smaller in volume and lighter in weight compared with other fuel cell types and the electrolyte is a solid material, therefore making the technology attractive for any conceivable application from powering a cell phone to a locomotive [1]. That is why most major automobile and electronic companies are competing in fuel cell development and why approximately 90% of fuel cell research and development work involves PEM fuel cells [2–4].

In the components of a PEM fuel cell, the bipolar plate has a high position. Its most important function is to supply reactant gases to the catalyst layers via the flow channel, and also to assist water and heat management. For several decades, many researchers have studied the flow channel design for improving the PEM fuel cell performance [5–10]. Various configuration designs of flow channel in PEM fuel cell systems such as the serpentine, parallel, and interdigitated channels were used for bipolar plates. The results of Refs. [11–13] suggested an interdigitated flow channel design. This flow channel has been provided to shorten the diffusion path for better mass transfer and convection flow in GDL for enhancing water removal capability and bringing about better performance, particularly at higher current densities.

The authors conducted the Taguchi methodology of quality control in the experimental analysis. Taguchi method is an efficient tool for the design of high-quality manufacturing system adopted in various fields extensively [14–16]. The target of Taguchi method is to reduce the variation (increasing robust) of the system performance with sources from a single characteristic's variation and revealing optimal setting by conducting a limited number of experiments with factor combinations. In recent years, much attention has been focused on the application of Taguchi method to PEM fuel cell designs. The results of applications indicated that

* Corresponding author. Tel.: +886 6 2747018x223; fax: +886 6 2747019.
E-mail address: z7708033@email.ncku.edu.tw (H.-W. Wu).

0378-7753/$ – see front matter © 2013 Elsevier B.V. All rights reserved.
http://dx.doi.org/10.1016/j.jpowsour.2013.01.020

Nomenclature

Symbol Description Units

A	area, m^2
ANOVA	analysis of variance, –
C	mole concentration, kmol m^{-3}
C_p	mixture-averaged specific heat capacity, J kg^{-1} K^{-1}
CF	correction factor, –
CI	confidence level, –
D	diffusivity of species, m^2 s^{-1}
E	voltage, V
F	Faraday's constant, 96,478 C mol^{-1}
f_e	degree of freedom (DOF), –
I	current, A
i	current density, A m^{-2}
j	exchange current density, A m^{-3}
k	thermal conductivity, W K^{-1} m^{-1}
K	permeability, m^2
l	levels, –
M	molecular weight, kg mol^{-1}
N	number, –
P	pressure, Pa
R_u	gas constant, 8.314 J mol^{-1} K^{-1}
S	source term, –
SS	sum of squares, –
S/N	signal-to-noise ratio, dB
T	temperature, K
$\vec{u}$	velocity vectors, m s^{-1}
W	power, W
X	mole fraction, –
Y	mass fraction, –
α	transfer coefficients, –
ε	porosity, –
ρ	density of gas, kg m^{-3}
μ	viscosity, m s^{-2}
κ	conductivity, Ω^{-1} cm^{-1}
ζ	stoichiometric flow ratio, –
η	overpotential, –
Δs	entropy charge, kJ mol^{-1} K^{-1}
Φ	phase potential, V

Superscript

sat	saturation
eff	effective, –

Subscript

a	anode, –
c	cathode, –
e	electric, –
i, j	species, –
m	ionic, –
s	solid phase, –
w	water, –

this technique obtained the optimum operating parameters and improved the performance of PEM fuel cells [17–20]. However, as the single-response problem is discussed in the previous section, one factor is very important to one quality characteristic while it may be unimportant to the other quality characteristics in the process of flow field designs. In addition, the flow field designs in the bipolar plate have been considered more crucial factors for enhancing the cell performance and decreasing the pressure drop losses. If more than one characteristic is simultaneously considered for the same process, the one factor method may not give a unique optimal combination of parameters; in particular, these characteristics compete with each other. The quality characteristic of the electric power in the Taguchi method has therefore been applied to the cell performance enhancement in the PEM fuel cell systems.

In the heat exchangers and gas turbine, rib, fin, groove or baffle was often employed to enhance the convective heat transfer rate leading to the compact heat exchange and increasing the efficiency [21–23]. The cooling or heating air passed the channel with several ribs to increase the powerful degree of cooling or heating levels over the smooth wall channel. Presently, several researchers [24–27] have illustrated the PEM fuel cell performance for single baffle plate, single rectangular block, or a row of baffle plates using a two-dimensional cathodic half cell model. However, the investigation was few on a row of rectangular parallelepipeds and the row arrangements at the axis in the anode and cathode channels to deflect the fluid and the performance enhancement. Therefore, this study presents flow modification by rows of rectangular parallelepipeds in the interdigitated flow channel in PEM fuel cells to ensure uniform reactant gas distribution and effective heat removal.

The above presented modification needs to introduce a new concept of robust parameter design at each trial of orthogonal array for simultaneous maximization of output power and minimization of pressure drop losses. Moreover, the numerical results are verified by the experiments using an experimental model with rectangular parallelepipeds. The results of this paper may be supplying the information to the engineers and researchers on the transport phenomenon of the novel interdigitated flow field and the optimum operation condition in PEM fuel cells.

2. Mathematical description

2.1. Modeling geometry and assumption

The three-dimensional model of an entire cell with rectangular parallelepiped rows is displayed in Fig. 1. This model considered the smooth-walled channel and rows of rectangular parallelepipeds crossed through the axis in the interdigitated flow channel of PEM fuel cells. The shapes in this schematic are used as follows: $H/H_1 = 1.5$, $H_2/H_1 = 0.5$, $H_3/H_1 = 0.6$. Table 1 lists the relational geometry and physical properties as well as parameters of fuel cell's components. The smooth-walled channel with rectangular parallelepiped numbers and their positions, which are regarded as the design variables, are plotted in Fig. 2. Fig. 2(a) shows the rectangular parallelepiped number of $N = 1$–9 in the interdigitated channel. In case I of Fig. 2(b), the rectangular parallelepiped number of $N = 8$ is uniformly located at the CHout (covering CHo1–CHo8). The case II is at the CHin (covering CHi1–CHi9), and the case III at the central position of CHo4 and CHo5.

The conservation equations including mass, momentum, species, charges, and energy were converted to a finite-volume method. An orthogonal uniform grid for computational discretion was involved in this work. The equations are developed through the following set of assumptions:

(a) The flow in a PEM fuel cell is treated as steady-state and laminar flow.
(b) The gas mixtures behave like perfect gas and incompressible flow.
(c) The diffusion layer, catalyst layer and membrane are considered each homogeneous and isotropic porous media.

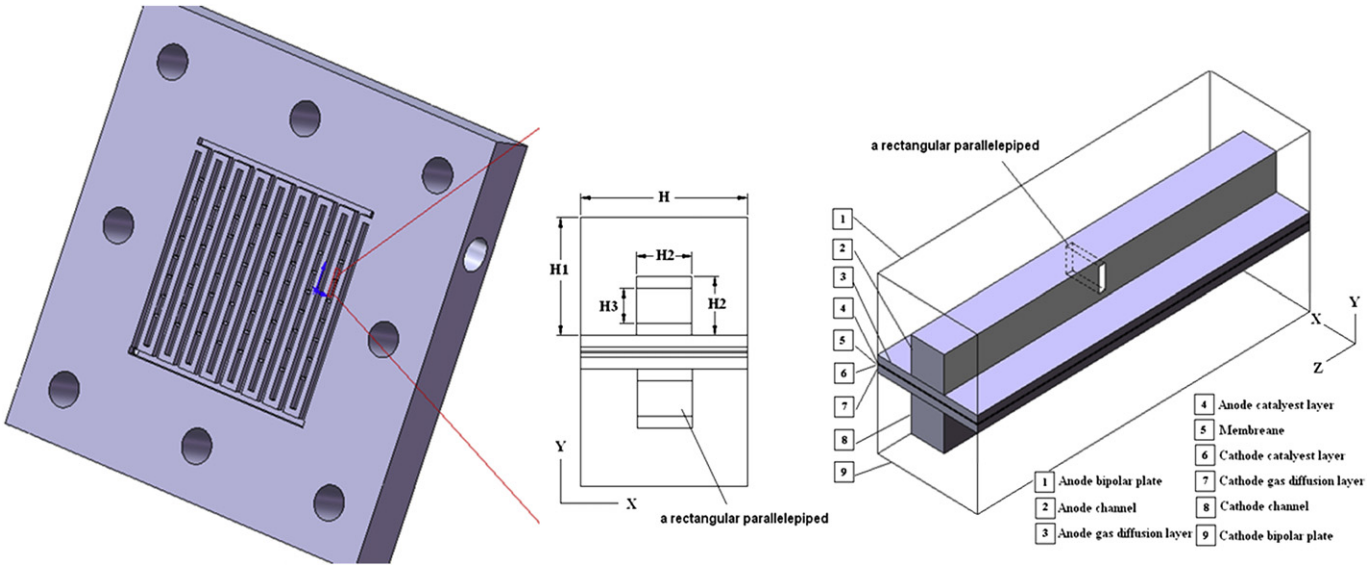

Fig. 1. Interdigitated channel design with rectangular parallelepipeds.

(d) Three species including oxygen, water, and nitrogen appear on the cathode side while only hydrogen and water exist on the anode side.
(e) Only proton is transported through the electrolyte, and the electron through the solid carbon phase.

2.2. Modeling equations

2.2.1. Gas flow channels

In the fuel cell channels, only the gas-phase is considered. The equations solved are [28]

Continuity equation: $$\nabla\cdot(\rho\vec{u}) = 0 \quad (1)$$

Momentum equation: $$\nabla\cdot(\rho\vec{u}\vec{u}) = -\nabla P + \nabla\cdot(\mu\nabla\vec{u}) \quad (2)$$

Energy equation: $$(\rho C_p)(\vec{u}\cdot\nabla T) = \nabla\cdot(k\nabla T) \quad (3)$$

Species transport equation: $$\nabla\cdot(\rho\vec{u}Y_i) = \nabla\cdot\left(\rho D_i^{\text{eff}}\nabla Y_i\right) \quad (4)$$

Table 1
The relational geometry and physical properties parameters in the interdigitated flow field.

Gas diffusion thickness	0.3 mm
Anode catalyst layer thickness	0.01 mm
Cathode catalyst layer thickness	0.01 mm
Membrane thickness	0.035 mm
Cell open-circuit voltage	1.0 V
Electronic conductivity	570 Ω^{-1} m^{-1}
Membrane permeability	1.8×10^{-18} m^2
Diffusion and catalyst layers permeability	1.76×10^{-11} m^2
Diffusion and catalyst layers porosity	0.4
Membrane porosity	0.28
H_2 diffusivity in the membrane (D_{m,O_2})	2.59×10^{-10} m^2 s^{-1}
O_2·H_2O diffusivity in the membrane (D_{m,O_2})	1.22×10^{-10} m^2 s^{-1}
H_2 diffusivity in anode gas channel	1.1028×10^{-4} m^2 s^{-1}
H_2O diffusivity in anode gas channel	1.1028×10^{-4} m^2 s^{-1}
O_2 diffusivity in cathode gas	3.2348×10^{-5} m^2 s^{-1}
H_2O diffusivity in cathode gas	7.35×10^{-5} m^2 s^{-1}
Operating pressure	101,325 Pa
Anode transfer coefficient (α_a)	2
Cathode transfer coefficient (α_c)	2

For PEM fuel cell operation, the second specie on anode side and cathode side is water vapor, which is assumed to exist at the saturation pressure. The mole fraction of water vapor is expressed as

$$X_w = \frac{P_w^{\text{sat}}(T)}{P} \quad (5)$$

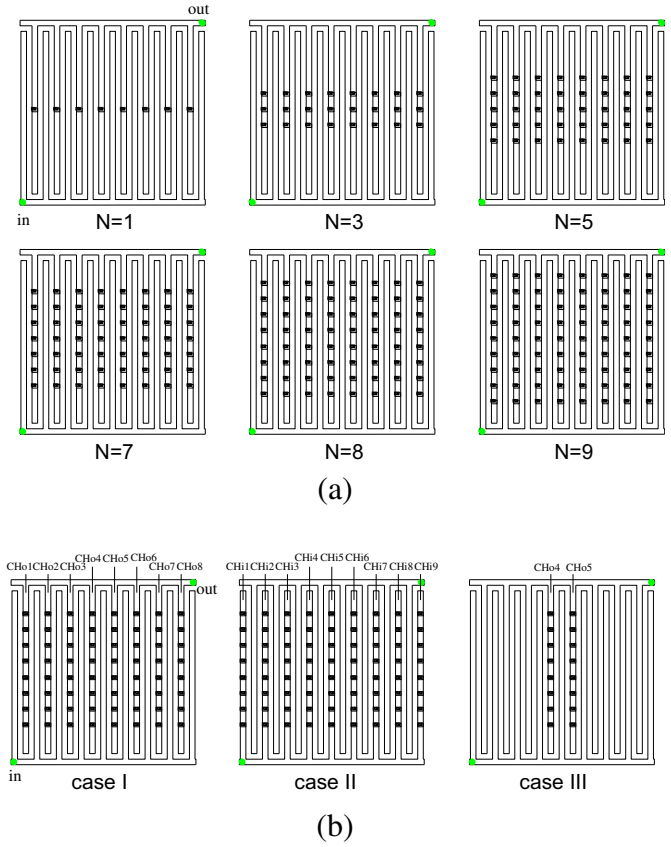

Fig. 2. The variation of (a) the rectangular parallelepiped number and (b) their positions in the interdigitated channel.

where the saturation pressure P_w^{sat} is given by

$$\log_{10}P_w^{sat}(T) = -2.1794 + 0.02953T - 9.1837T^2 + 1.4454T^3 \quad (6)$$

The sum of all mass fractions is notably equal to unity

$$\sum Y_i = 1 \quad (7)$$

2.2.2. Porous medium

The equations that govern the transport phenomena in the diffusion layers, catalyst layers, and membrane are similar to the channel equations, except that the gas-phase porosity ε of the material is introduced into the generic advection–diffusion equation.

Continuity equation: $$\nabla\cdot(\varepsilon\rho\vec{u}) = 0 \quad (8)$$

Momentum equation: $$\nabla\cdot(\varepsilon\rho\vec{u}\vec{u}) = -\varepsilon\nabla P + \nabla\cdot(\varepsilon\mu\nabla\vec{u}) - S_m \quad (9)$$

Energy equation: $$(\varepsilon\rho C_p)(\vec{u}\cdot\nabla T) = \nabla\cdot(k\nabla T) + S_T \quad (10)$$

Species transport equation: $$\nabla\cdot(\varepsilon\rho\vec{u}Y_i) = \nabla\cdot\left(\rho D_i^{eff}\nabla Y_i\right) + S_i \quad (11)$$

By the Bruggman correlation to consider porosity and tortuosity influencing porous electrodes and membrane, this study changes the effective mass diffusion coefficient by the following equation [29].

Gas diffusion coefficient in porous media

$$D_i^{eff} = D_i\varepsilon^{1.5} \quad (12)$$

Diffusivity in the gas channels

$$D_i(T,P) = D_{0,i}\left(\frac{T}{T_0}\right)^{1.5}\left(\frac{P_0}{P}\right) \quad (13)$$

The pressure and temperature dependencies in Eq. (13) are from an empirical relation and the dependencies on the porosity (i.e., volumetric fraction available for fluid flow). In addition, liquid water saturation in the porous gas diffusion and catalyst layers is taken into account not only the volumetric fraction available for gas flow but also the tortuosity of the porous media using the effective medium theory. For a three-component gas, there are four independent Fick diffusion coefficients. Values of the binary diffusion coefficients are given in Table 1.

2.2.2.1. Charge equation. In the catalyst layers and membrane, using Ohmic's law, the potential equations for solid and electrolyte phases are written as follows:

$$\nabla\cdot(-\kappa_s\nabla\Phi_s) = S_{\Phi s} \quad (14)$$

$$\nabla\cdot(-\kappa_e\nabla\Phi_e) = S_{\Phi e} \quad (15)$$

Table 2 shows the corresponding source terms in the governing equations for the diffusion layers, catalyst layers, and membrane. In the momentum equations, the source terms are calculated according to the Darcy law [30] illustrating an extra drag force, which is proportional to the fluid viscosity and velocity, and inversely proportional to the porous material's permeability. The possible heat sources in the energy equation are then the cause of Ohmic resistance through solid in pores. In the table, employing

Table 2
The source terms of governing equations.

	S_m	S_i	S_T	S_Φ
CH	0	0	0	0
GDL	$-\frac{\mu}{K}\varepsilon\vec{u}$	0	$\frac{i_e^2}{\kappa_s}$	0
CL	$-\frac{\mu}{K}\varepsilon\vec{u}$	$H_2 = -j_a M_{H_2}/2F$ $O_2 = j_c M_{O_2}/4F$ $H_2O = -j_c M_{H_2O}/2F$	$\left[\frac{T(-\Delta s)}{n_e F}+\eta\right]\cdot j$	j
MEM	$-\frac{\mu}{K}\varepsilon\vec{u}$	0	$\frac{i_m^2}{\kappa_m}$	–

Bulter–Volmer [31] expression obtains the j_a and j_c of the exchange current density at anode side and cathode side

$$j_a = j_0^{ref}\left(\frac{C_{H_2}}{C_{H_2}^{ref}}\right)^{1/2}\cdot\left[\exp\left(\frac{\alpha_a F}{R_u T}\eta_a\right) - \exp\left(-\frac{\alpha_c F}{R_u T}\eta_a\right)\right] \quad (16)$$

$$j_c = -j_0^{ref}\left(\frac{C_{O_2}}{C_{O_2}^{ref}}\right)\cdot\left[\exp\left(\frac{\alpha_a F}{R_u T}\eta_c\right) - \exp\left(-\frac{\alpha_c F}{R_u T}\eta_c\right)\right] \quad (17)$$

where α is the transfer coefficients, η the activation overpotential, and j_0^{ref} the reference exchange current density.

$$\eta_a = \Phi_m - \Phi_{s,a}$$

$$\eta_c = \Phi_{s,c} - \Phi_m - E_0$$

where E_0 is the open-circuit voltage.

2.2.3. Bipolar plates

The primary function of bipolar plates is to transfer electrons toward the gas diffusion layers and to the reaction sites. Hence, only the energy equation is considered in the solid plates

$$\nabla k\cdot\nabla T = 0 \quad (18)$$

2.3. Boundary conditions

In this paper, the mass flow inlet boundary conditions are described by a stoichiometric flow ratio, ζ, defined by

$$u_{in,i} = \zeta\frac{i}{N_e F}\frac{A_{MEA}}{A_{CH}}\frac{1}{X_i}\frac{R_u T}{P_i} \quad (19)$$

For convenience, the stoichiometric flow ratios defined in Eq. (19) refer to the current density of 1 A cm^{-2} here, and the ratios are regarded as dimensionless flow rates of the fuel and oxidant.

At the outlet boundary conditions, only the pressure is being defined in the flow channel, and the gradient of all other variables in the flow direction assumed to be zero. In the z direction of the MEA, zero normal gradients are prescribed as well as zero normal fluxes of any transported parameter $\partial\Phi/\partial z = 0$. On the bipolar plates (y-direction), boundary conditions need only to be given for the energy equation. This can be done in the form of either a heat flux or a temperature value, or a mixture of the above. Currently, symmetry is assumed at the outer y-boundaries leading to a no-heat-flux boundary condition $\partial T/\partial y = 0$. As the membrane/catalyst interface is assumed to be impermeable to gases, the flux of gases is zero at this interface $\partial C/\partial x = 0$. The same condition is imposed on the surface of metal electrodes.

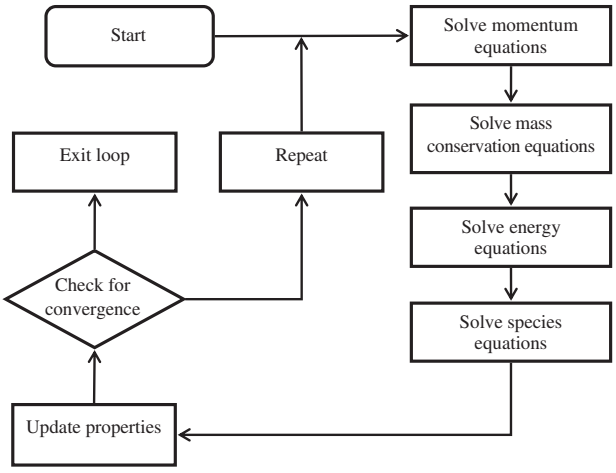

Fig. 3. Solving procedure of the numerical algorithm.

2.4. Numerical method

All model equations containing mass, momentum, species, temperature, and charges were converted to a finite difference form by the control volume method [32]. The flow diagram for this numerical algorithm is shown in Fig. 3. The SIMPLE (semi-implicit method for pressure-linked equations) scheme [33] was adopted for the pressure correction. For nonlinear problem, this study used the inlet mass fractions and velocities as an initial guess. First, the momentum equations are solved in the x, y, and z directions. A pressure correction equation is then applied to revise the mass conservation and to calculate the velocities. Next, using the energy equation estimates the temperature for an entire cell, and the electrochemical reactions for the heat generation. Last, the mass fractions of species are employed to compute the mixture properties in the control volume. All equations are solved iteratively until the relative error reached to a convergent value when the residuals of serial iterations are less than 10^{-6} for all variables. The seven runs were examined by variant hexahedral meshes of 340,000–920,000 cells in the computational domain at 0.4 V as illustrated in Fig. 4(a). There was a slight variation in current density at 0.4 V until the change in numerical results is within tolerance of 0.2%. The mesh of 840,000 cells was therefore employed in the following calculations. Contrast of the experimental and numerical

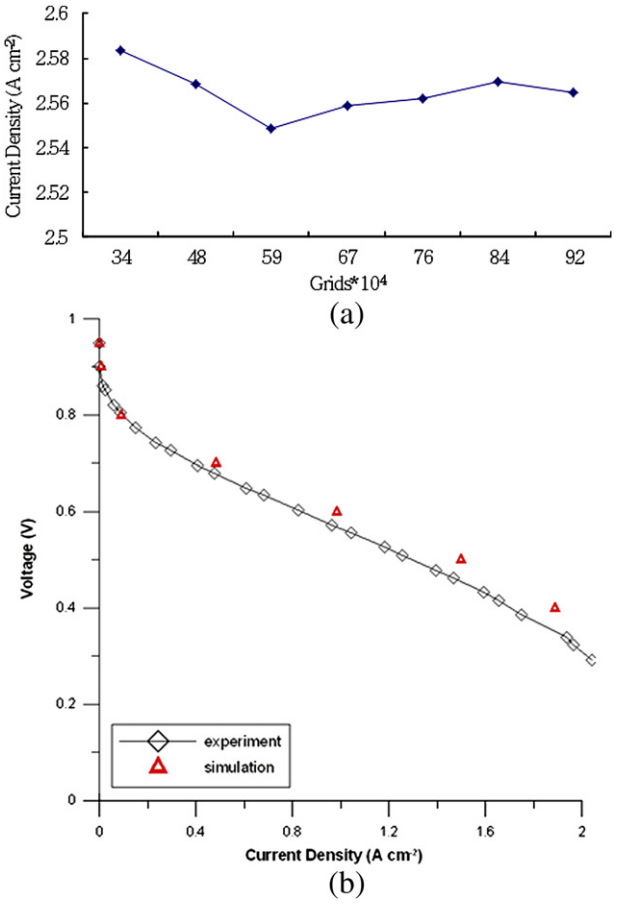

Fig. 4. Comparison of prediction results with (a) various grids and (b) the experiment.

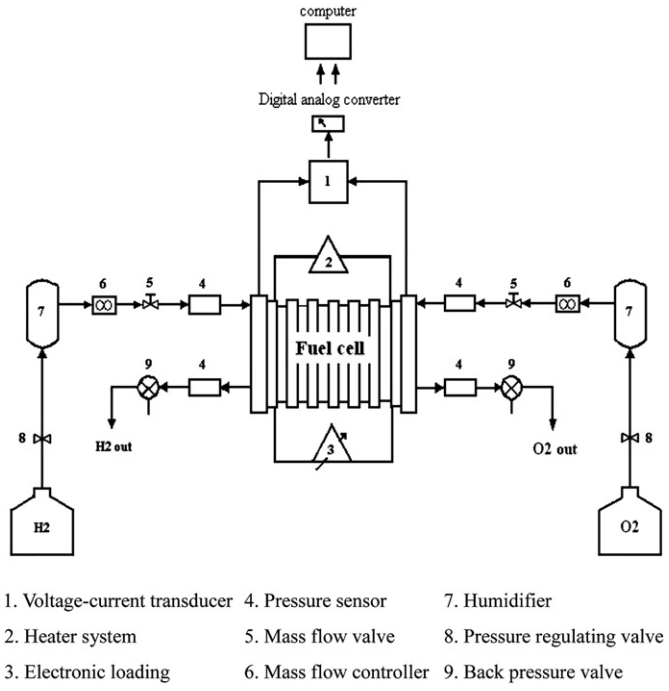

Fig. 5. Schematic of experimental setup.

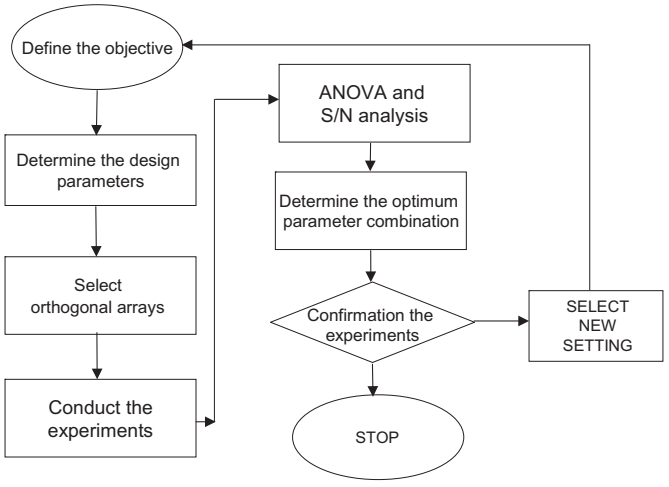

Fig. 6. Flow chart of the Taguchi method.

results validates the prediction of PEM fuel cell performance as indicated in Fig. 4(b).

3. Experimental system and approach

3.1. Experimental system

In the fuel cell experimental system, the chief features of equipment are shown in Fig. 5. The test station consists of an electronic load system and the subsystems, which contain mass flow controllers, temperate controllers, humidifiers, pressure instrumentation, and back pressure controllers for the reactant gases. The 300 W electronic loads used in these experiments have a combined maximum current of 60 A, and a voltage range of 0–50 V. A PEM fuel cell is composed of bipolar plates with 1.5 × 1.5 mm interdigitated flow channels and a membrane electrode assembly (MEA) with 25 cm^2 active surface area in this study. Using the instruments measures the current (I), voltage (E), and power (W), and the current is measured for each period of 60 s.

3.2. Experimental approach

In the late 1940s, Taguchi developed a new method to reduce the variation and to investigate how different parameters affect the process through design of experiments [34]. Furthermore, this method applied orthogonal arrays to allocate parameters instead of test all possible combinations for reducing the experimental frequency. Consequently, this paper used Taguchi method to explore how operational parameters influence the PEM fuel cell performance in modified interdigitated flow field design. The procedure of Taguchi method is described in detail as follows in Fig. 6. This procedure starts defining the objective to determine the design parameters. After determining the design parameters and selecting the orthogonal array, to conduct experiments obtains data. For executing the ANOVA and S/N analysis, to use the data finds out the optimum parameter combination. The final step is to run a confirmation experiment to verify the experimental results. If this confirmation experiment fails, the new setting has to be selected and the procedure is repeated until the confirmation experiment succeeds.

In this work, the desired design for PEM fuel cell is to achieve the best performance of the maximum output power and minimum pressure drop under given conditions. The conditions involve the cell temperature, anode humidifier temperature, cathode humidifier temperature, anode stoichiometric ratio, and cathode stoichiometric ratio. Then there are five control factors (N_f) and each is changed for three levels (l) in selecting an appropriate orthogonal array. As a result, the minimum number of experiments in the array is

$$N = (l-1) \times N_f + 1 \tag{20}$$

The Taguchi method employs a signal-to-noise (S/N) ratio to quantify the variation of performance of an output characteristic.

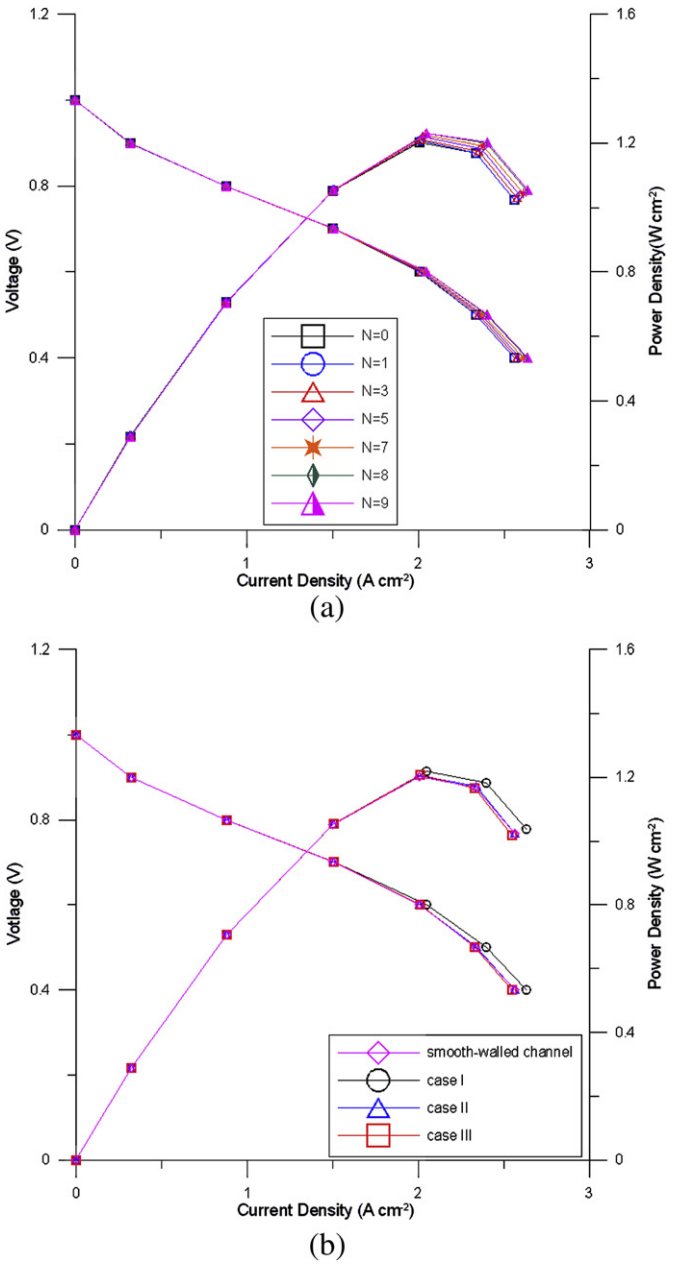

Fig. 7. Cell performance of various designs: (a) the rectangular parallelepiped numbers and (b) their positions.

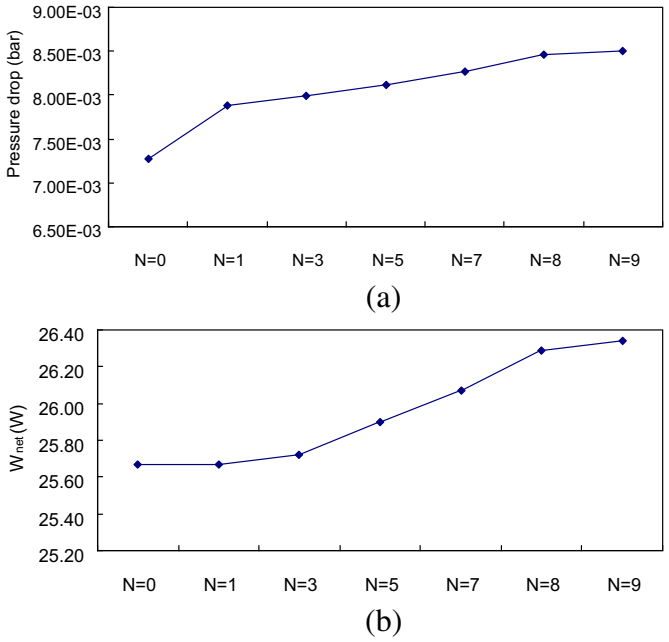

Fig. 8. Comparative results of (a) the pressure drops and (b) the net power in various rectangular parallelepiped numbers.

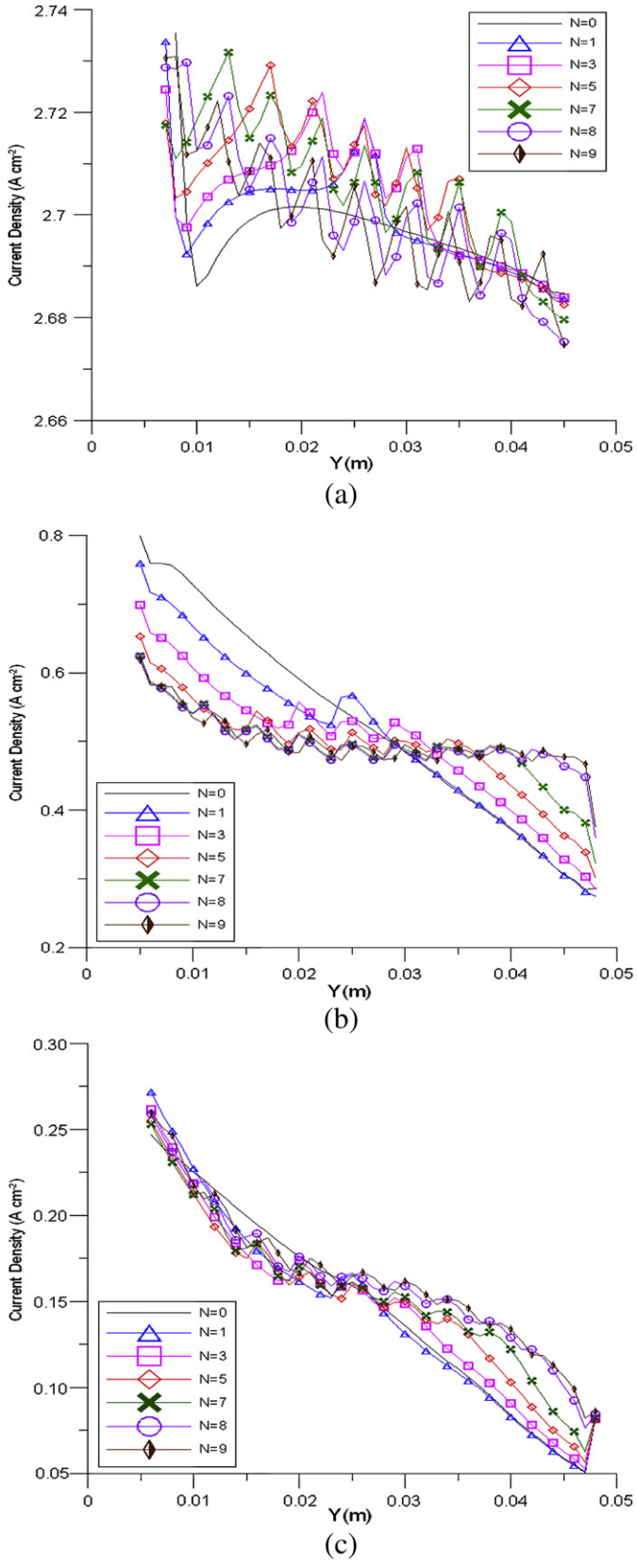

Fig. 9. The local current density profile of rectangular parallelepiped rows along (a) CHo1, (b) CHo4, and (c) CHo8 between the GDL and CL.

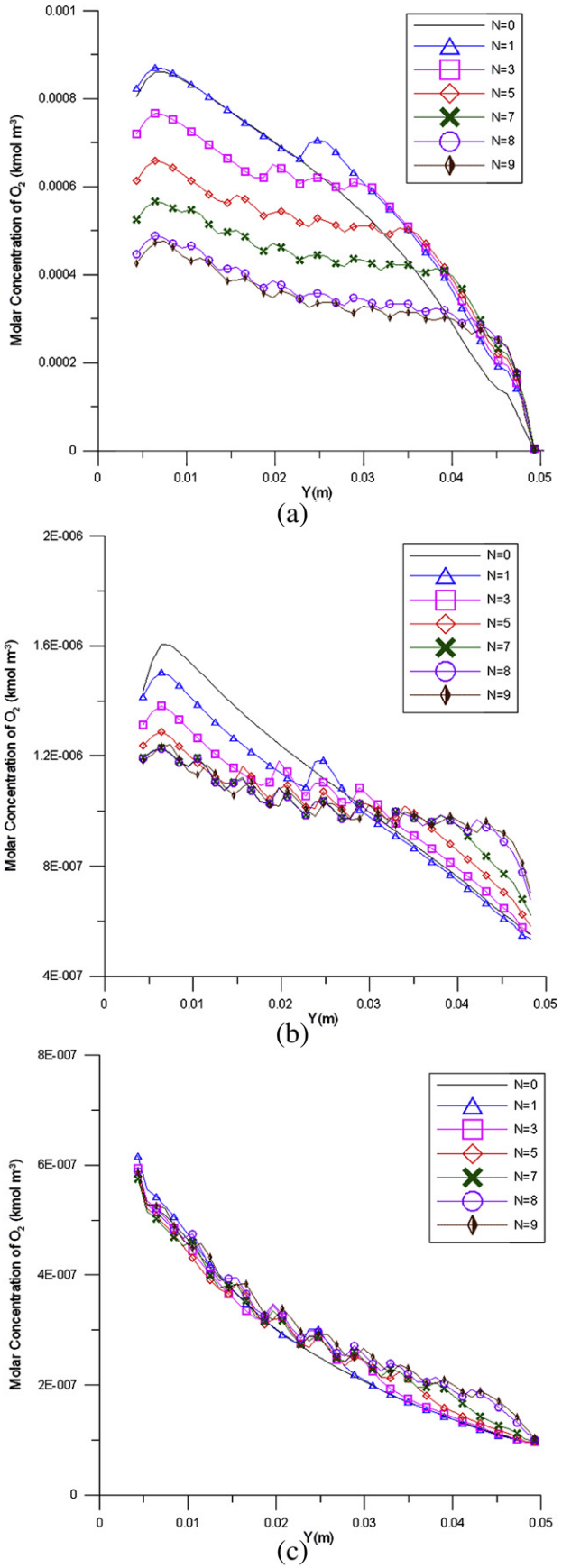

Fig. 10. The oxygen concentration distribution profile of rectangular parallelepiped rows along (a) CHo1, (b) CHo4, and (c) CHo8 between the GDL and CL.

In the experiment, the net power belongs to the larger-the-better quality characteristics in Eq. (21).

$$S/N_{\mathrm{LTB}} = -10 \times \log\left(\frac{1}{N}\sum_{i=1}^{N}\frac{1}{y_i^2}\right) \tag{21}$$

where N is the test number and y_i is the quality characteristic value evaluated by a trial.

The average S/N responses for each factor levels are computed in the orthogonal arrays. An analysis of variance (ANOVA) is the statistical methodology to identify the significant effect of each controlled factor and their interactions on the experimental results. The term variation is indicated by several mathematical descriptions as follows:

$$\text{Total sum of squares}: \quad \mathrm{SS}_T = \sum_{i=1}^{N}\left(y_i^2 - \mathrm{CF}\right) \tag{22}$$

where CF is the correction factor

$$\mathrm{CF} = \left(\sum_{i=1}^{N} y_i\right)^2 \Big/ N$$

The total and factor sums of squares are the basic computations needed for ANOVA. Other quantities calculated as parts of the ANOVA table information are all derived from the original sums of squares. For the factor A, they are used as follows:

$$\text{Mean variance}: \quad V_A = \frac{S_A}{f_A} \tag{23}$$

$$F-\text{ratio}: \quad F_A = \frac{V_A}{V_e} \tag{24}$$

$$\text{Pure sum of squares}: \quad SS'_A = \mathrm{SS}_A - (V_e \times f_A) \tag{25}$$

$$\text{Percent contribution}: \quad \rho_A = \frac{\mathrm{SS}'_A}{\mathrm{SS}_T} \tag{26}$$

where V_e is the variance of the error term (obtained by computing the error sum of squares and divided by error degrees of freedom) and f_A is the degrees of freedom (DOF) of factor A.

Finally, the predicted optimal parameter combinations are validated by a confirmatory experiment as follows:

$$\mathrm{CI} = \sqrt{F(\alpha,1,f_e)V_e\left[\frac{1}{N_{\mathrm{eff}}}+\frac{1}{R}\right]}, \quad N_{\mathrm{eff}} = \frac{N}{1+f_T} \tag{27}$$

where $F(\alpha,1,f_e)$ is the F-ratio required for $100(1-\alpha)$ percent confidence level; f_e DOF for error; V_e error variance; R number of replications of confirmation experiment; N_{eff} effective number of replications; N the total number of experiments, and f_T the total DOF for the estimate of mean optimum.

4. Results and discussion

4.1. Effects of the rectangular parallelepiped numbers and arrangements in the channels

The authors applied the simulation to realize various influences of the rectangular parallelepiped numbers and arrangements on the PEM fuel cell performance in the interdigitated channel. Fig. 7(a) displays the cell performances at the voltage below 0.5 V strongly varying with various numbers of rectangular parallelepiped. The cell performance is enhanced with an increase in the number of rectangular parallelepipeds. The fuel gases are forced to flow into the gas diffusion layer and catalyst layer to enhance the possibility of chemical reaction occurring at the catalyst layer. The output power of case III is greater than that of smooth-walled channel from 25.70 W to 26.32 W at 0.4 V. Fig. 7(b) explores three types of rectangular parallelepiped rows with various

Table 3
Experimental results and S/N ratios.

Exp.	A	B	$A\times B$	$A\times B$	C	$A\times C$	$A\times C$	$B\times C$	D	E	$B\times C$	e	e	W_{net} (W)				MSD	S/N
1	1	1	1	1	1	1	1	1	1	1	1	1	1	13.69	13.70	13.67	13.66	5.34E-03	22.72
2	1	1	1	1	2	2	2	2	2	2	2	2	2	14.31	14.33	14.34	14.37	4.86E-03	23.13
3	1	1	1	1	3	3	3	3	3	3	3	3	3	16.07	15.93	15.91	15.91	3.93E-03	24.06
4	1	2	2	2	1	1	1	2	2	2	3	3	3	16.56	16.57	16.57	16.58	3.64E-03	24.39
5	1	2	2	2	2	2	2	3	3	3	1	1	1	14.33	14.51	14.54	14.55	4.77E-03	23.22
6	1	2	2	2	3	3	3	1	1	1	2	2	2	16.30	16.29	16.28	16.29	3.77E-03	24.24
7	1	3	3	3	1	1	1	3	3	3	2	2	2	16.09	16.09	16.12	16.11	3.86E-03	24.14
8	1	3	3	3	2	2	2	1	1	1	3	3	3	15.52	15.54	15.54	15.60	4.14E-03	23.83
9	1	3	3	3	3	3	3	2	2	2	1	1	1	17.26	17.25	17.18	17.16	3.38E-03	24.72
10	2	1	2	3	1	2	3	1	2	3	1	2	3	16.91	16.91	16.90	16.89	3.50E-03	24.56
11	2	1	2	3	2	3	1	2	3	1	2	3	1	16.32	16.33	16.31	16.32	3.75E-03	24.25
12	2	1	2	3	3	1	2	3	1	2	3	1	2	18.91	18.91	18.94	18.98	2.79E-03	25.55
13	2	2	3	1	1	2	3	2	3	1	3	1	2	18.09	18.04	18.01	17.99	3.08E-03	25.12
14	2	2	3	1	2	3	1	3	1	2	1	2	3	18.49	18.49	18.49	18.50	2.92E-03	25.34
15	2	2	3	1	3	1	2	1	2	3	2	3	1	18.24	18.25	18.25	18.25	3.00E-03	25.22
16	2	3	1	2	1	2	3	3	1	2	2	3	1	20.10	20.14	20.13	20.13	2.47E-03	26.07
17	2	3	1	2	2	3	1	1	2	3	3	1	2	21.04	21.02	21.01	21.01	2.26E-03	26.45
18	2	3	1	2	3	1	2	2	3	1	1	2	3	17.51	17.54	17.53	17.53	3.25E-03	24.88
19	3	1	3	2	1	3	2	1	3	2	1	3	2	12.20	12.14	12.11	12.07	6.79E-03	21.68
20	3	1	3	2	2	1	3	2	1	3	2	1	3	14.55	14.52	14.53	14.54	4.73E-03	23.25
21	3	1	3	2	3	2	1	3	2	1	3	2	1	16.30	16.30	16.31	16.31	3.76E-03	24.25
22	3	2	1	3	1	3	2	2	1	3	3	2	1	15.97	15.83	15.80	15.75	3.99E-03	23.99
23	3	2	1	3	2	1	3	3	2	1	1	3	2	16.24	16.26	16.20	15.90	3.83E-03	24.16
24	3	2	1	3	3	2	1	1	3	2	2	1	3	18.67	18.64	17.89	17.55	3.03E-03	25.18
25	3	3	2	1	1	3	2	3	2	1	2	1	3	15.59	15.53	16.51	17.51	3.80E-03	24.20
26	3	3	2	1	2	1	3	1	3	2	3	2	1	21.48	21.45	21.42	21.37	2.18E-03	26.62
27	3	3	2	1	3	2	1	2	1	3	1	3	2	19.53	19.49	19.46	19.41	2.64E-03	25.79

positions how to influence the cell performance. The case I is the rectangular parallelepiped rows at the CHout (covering CHo1–CHo8), the case II at the CHin (covering CHi1–CHi9), and the case III at the CHo4 and CHo5. The cell performance of smooth-walled channel is obviously worse than that of the case I and the case II and case III have the same trend with case I.

However, the cell performance increases with an increase in the rectangular parallelepiped numbers and the pressure drops do too. The higher pressure drop usually induces the higher pumping power from the reactant gases inlet. Hence, the authors consider the effects of pressure drop in this modified interdigitated flow field design. In Fig. 8, rectangular parallelepiped numbers affect the pressure drop, $\Delta P' = P'_{in} - P'_{out}$, and the net power [35], $W_{net} = W_{FC} - W_{\Delta P'}$. Total pressure drops rise with increasing the rectangular parallelepiped number but slow down at N larger than 8, which the gap of $N = 8$–9 is only 0.5% in Fig. 8(a). The electrical powers of the various rectangular parallelepiped numbers are far larger than the pressure drop losses and agree with the net power (Fig. 8(b)). In all cases, the rectangular parallelepiped number of $N = 9$ has the maximum net power (W_{net}) and the pressure drop larger than the smooth-walled channel does by 0.001 bar. Then the net power of $N = 8$ is close to $N = 9$ about 0.05 W.

4.2. Effects of the local distributions of the rectangular parallelepiped numbers

Fig. 9 indicates the local current density profiles of rectangular parallelepiped rows along CHo1, CHo4, CHo8 between the GDL and CL at 0.4 V. In the figure, each hump region is induced by the interactions of flow fields and the deflection effect for the rectangular parallelepiped-to-rectangular parallelepiped to enhance the electrochemical reaction and to have more uniform current density distributions. As shown in Fig. 9(a), the local current density rises with an increase in the rectangular parallelepiped number and larger at the CHo1 downstream than at the smooth-walled channel. At the mid channel of flow field as the CHo4, the local current density with the smooth-walled channel and the rectangular parallelepiped number of N smaller than 5 cuts down quickly from 0.8 A cm^{-2} to 0.3 A cm^{-2}, and N larger than 5 has more uniform current density distributions as indicated in Fig. 9(b). In Fig. 9(c), the local current density of $N = 1$ is similar to that of the smooth-walled channel ones and $N = 8$ is like $N = 9$.

The local distribution of oxygen concentration profiles of rectangular parallelepiped rows is shown in Fig. 10 along CHo1, CHo4, CHo8 between the GDL and CL at 0.4 V. Fig. 10(a) and (b) displays that the oxygen concentration distribution is more uniform with increasing the rectangular parallelepiped number in the first to mid channels of full flow field as CHo1–CHo4. There is the slow depletion of the oxygen concentrations along the final channel (CHo8) as shown in Fig. 10(c). Anyway, the local current density and oxygen distributions of $N = 8$ are similar to those of $N = 9$. Therefore, the authors select the rectangular parallelepiped number of $N = 8$ and arrangement at the CHout, the case I, as a novel design, make it by the electrical discharge machining and optimize the operating parameters of PEM fuel cell by Taguchi method.

4.3. Experimental analysis of the Taguchi method for the novel model

This study applied the L_{27} orthogonal array of the Taguchi method to select temperature of a fuel cell (A), anode humidification temperature (B), cathode humidification temperature (C), stoichiometric flow ratio of hydrogen (D), and stoichiometric flow ratio of oxygen (E), as the operating factors for the novel interdigitated flow field design with the rectangular parallelepiped number ($N = 8$) and arrangement (case I). Three levels of

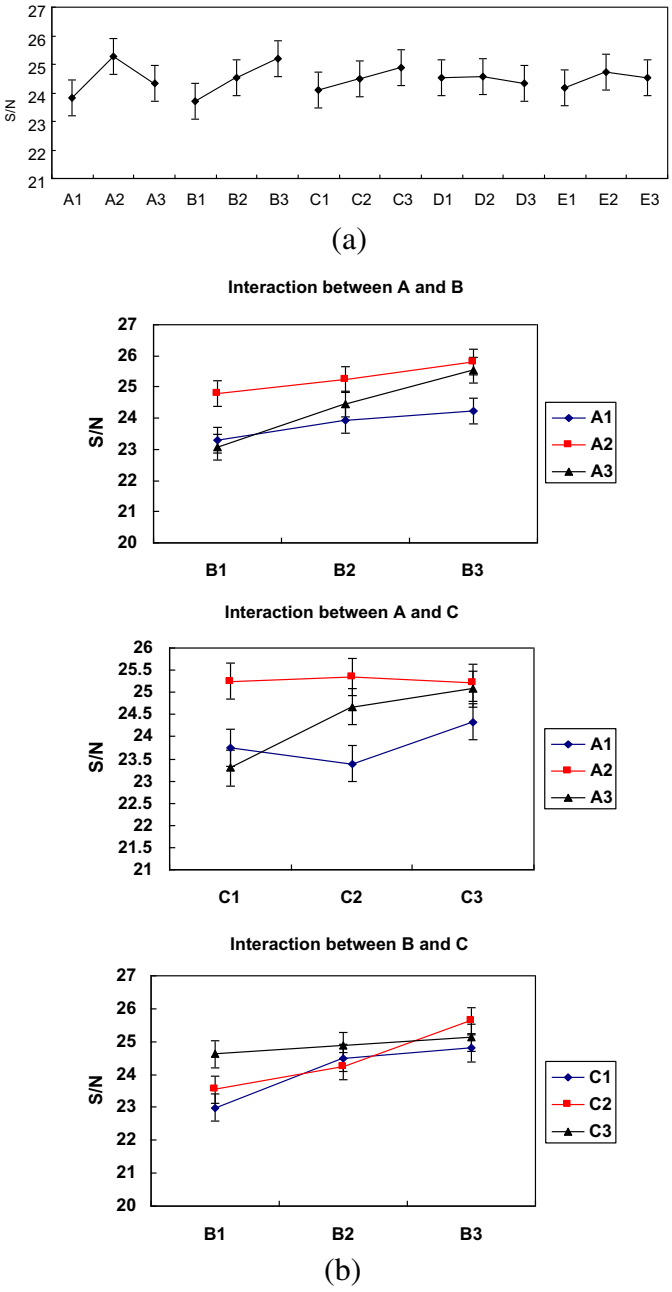

Fig. 11. S/N responses for (a) the net power and (b) the interactions of $A \times B$, $A \times C$, and $B \times C$.

Table 4
ANOVA for the L_{27} (3^{13}) design.

Factor	SS	DOF	Var	F	$F_{0.05}$	SS′	Contribution (%)
A	9.65	2	4.82	57.10	5.14	9.48	28.33
B	9.81	2	4.90	58.06	5.14	9.64	28.82
C	2.72	2	1.36	16.12	5.14	2.55	7.64
D	(0.24)	(2)	–	–	–	–	–
E	1.42	2	0.71	8.39	5.14	1.25	3.73
AB	2.36	4	0.59	6.97	4.53	2.02	6.03
AC	3.92	4	0.98	11.60	4.53	3.58	10.71
BC	3.07	4	0.77	9.10	4.53	2.74	8.18
e	(0.26)	(4)	–	–	–	–	–
Error	0.51	6	0.08	S=	0.29 dB	2.20	6.57
Total	33.45	26	At least 95% confidence			33.45	100.00

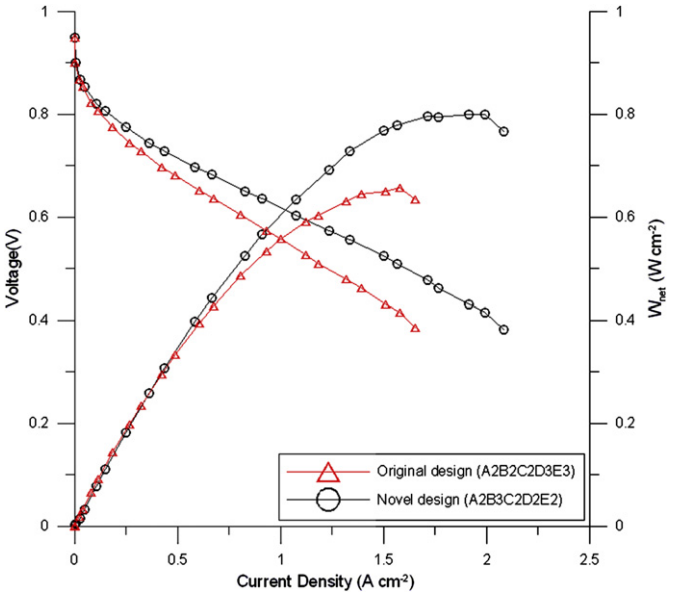

Fig. 12. Compared polarization curves between the original design of the smooth-walled channel at the optimum parametric combinations of $A_2B_2C_2D_3E_3$ and the novel design of the case I at $A_2B_3C_3D_2E_2$.

temperature are 313 K, 333 K, and 353 K and three levels for stoichiometric flow ratio are 1.2, 1.9, and 2.7. The quality characteristic is to set the net electric power representing the cell performance and the related *S*/*N*s as shown in Table 3. Fig. 11(a) is the average *S*/*N* responses of each factor level variation and the highest ones express the optimum combination of the maximum net power as $A_2B_3C_3D_2E_2$.

With the optimum combination of process parameters, an analysis of variance (ANOVA) finds out the most important factors and quantifies their effects as listed in Table 4. In addition, the authors considered the effect of the interactions between factors *A*, *B*, and *C*. An ANOVA indicates the control factors *A*, *B*, *C*, and *E*, and the interactions of $A \times B$, $A \times C$, and $B \times C$ with significant effects for obtaining the maximum net power as shown in Fig. 11(b). The optimum parametric combination is therefore set by $A_2B_3C_2D_2E_2$ of 19.3 W based on the results of the interactions.

To confirm the statistical predicted results of Taguchi method, four replications have been run. The average *S*/*N* from the confirmation experiments is 25.72 dB to fall in the predicted optimum parametric combination of 26.23 ± 0.63 dB at the 95% confidence level. Hence, the predictions of Taguchi methodology are verified to agree with the confirmation results. Consequently, this design improves the cell performance, and the authors make it possible to compare experimental results with those obtained in three-dimensional simulations at the same conditions. This comparison shows that the numerical and experimental results are in close agreement. The experimental results indicate the net power of the novel design, case I, more than that of the original one, the smooth-walled channel, by approximately 26% in the optimum parameter combination as displayed in Fig. 12. The optimum parametric combination of the original design is set by $A_2B_2C_2D_3E_3$ of 16.43 W and that of the novel design is set by $A_2B_3C_3D_2E_2$ of 20.67 W based on the experimental analysis of Taguchi method.

5. Conclusion

The novel design of the rectangular parallelepiped numbers and arrangements in the interdigitated flow field was developed to augment the performance of a PEM fuel cell by simulation and experiment. The simulation results show how the rectangular parallelepiped number and arrangements affect the polarization curves, the pressure drop, the net power, the local distributions of current density, and oxygen concentrations. The novel design of the interdigitated flow field is obtained by the rectangular parallelepiped number of $N = 8$ and arrangement in the CHout, and it also has the better electric power. To explore the operational parameters influencing the performance of PEM fuel cells comprehends the actual variation between the novel design and the smooth-walled channel. The study therefore applies the experiment by the L_{27} orthogonal array of the Taguchi method to the novel design to determine the optimum parameter combination. The ANOVA method indicates the control factors *A*, *B*, *C*, and *E*, and the interactions of $A \times B$, $A \times C$, and $B \times C$ with significant effects for obtaining the maximum net power. At 0.4 V, the net power of this design at the optimum parameter combination of $A_2B_3C_2D_2E_2$ is 26% more than that of the smooth-walled channel at the $A_2B_2C_2D_3E_3$.

Acknowledgments

The authors are really thankful to the National Science Council ROC for the financial offer granted by 97-2221-E-006-270-MY3.

References

[1] Xianguo Li, Principles of Fuel Cells, Taylor & Francis Group, New York, 2006.
[2] A. Contreras, F. Posso, E. Guervos, Appl. Energy 87 (2010) 1376–1385.
[3] Frano Barbir, PEM Fuel Cells: Theory and Practice, Elsevier Academic Press, 2005.
[4] M.A.J. Cropper, S. Geiger, D.M. Jollie, J. Power Sourc. 131 (2004) 57–61.
[5] Peng Hu, Linfa Peng, Weigang Zhang, Xinmin Lai, J. Power Sourc. 187 (2009) 407–414.
[6] Xianguo Li, Imran Sabir, Int. J. Hydrogen Energy 30 (2005) 359–371.
[7] C. Xu, T.S. Zhao, Electrochem. Commun. 9 (2007) 497–503.
[8] C.T. Wang, Y.C. Hu, P.L. Zheng, Appl. Energy 87 (2010) 1366–1375.
[9] Suman Basu, Chao-Yang Wang, Ken S. Chen, Chem. Eng. Sci. 65 (2010) 6145–6154.
[10] J.P. Owejan, T.A. Trabold, D.L. Jacobson, M. Arif, S.G. Kandlikar, Int. J. Hydrogen Energy 32 (2007) 4489–4502.
[11] Lin Wang, Hongtan Liu, J. Power Sourc. 134 (2004) 185–196.
[12] Wei-Mon Yan, Chi-Yen Chen, Sheng-Chin Mei, Chyi-Yeou Soong, Falin Chen, J. Power Sourc. 162 (2006) 1157–1164.
[13] Jiin-Yuh Jang, Chin-Hsiang Cheng, Yu-Xian Huang, Int. J. Heat Mass Transf. 53 (2010) 732–743.
[14] S. Maghsoodloo, J. Qual. Technol. 22 (1990) 57–67.
[15] Ranjit K. Roy, A Primer on the Taguchi Method, Society of Manufacturing Engineers, 1990.
[16] G. Taguchi, Y. Yokoyama, Y. Wu, Taguchi Methods: Design of Experiments, ASI Press, Chicago, 1993.
[17] Koan-Yuh Chang, Int. J. Hydrogen Energy 36 (2011) 13683–13694.
[18] Wei-Lung Yu, Sheng-Ju Wu, Sheau-Wen Shah, Int. J. Hydrogen Energy 35 (2011) 11138–11147.
[19] Shan-Jen Chen, Jr-Ming Miao, Sheng-Ju Wu, Renew. Energy 39 (2012) 250–260.
[20] Nita Solehati, Joonsoo Bae, Agua P. Sasmito, J. Ind. Eng. Chem. 18 (2012) 1039–1050.
[21] W.M. Yan, S.C. Mei, Int. J. Heat Mass Transf. 49 (2006) 159–170.
[22] M.E. Taslim, Int. J. Heat Exchangers 6 (2005) 135–152.
[23] Pongjet Promvonge, Chinaruk Thianpong, Int. Commun. Heat Mass Transf. 35 (2008) 1327–1334.
[24] Hui-Chung Liu, Wei-Mon Yan, Chyi-Yeou Soong, Falin Chen, J. Power Sourc. 142 (2005) 125–133.
[25] C.Y. Soong, Wei-Mon Yan, C.-Y. Tseng, H.C. Liu, Falin Chen, H.S. Chu, J. Power Sourc. 143 (2005) 36–47.
[26] Shiang-Wuu Perng, Horng-Wen Wu, J. Power Sourc. 175 (2008) 806–816.
[27] Shiang-Wuu Perng, Horng-Wen Wu, Tswen-Chyuan Jue, Kuo-Chih Cheng, Appl. Energy 86 (2009) 1541–1554.
[28] Robert Byron Bird, Warren E. Stewart, Transport Phenomena, Wiley, New York, 2007.
[29] J. Bear, J.M. Buchlin, Modeling and Application of Transport Phenomena in Porous Media, Kluwer Academic Publishers, Boston, MA, 1991.
[30] S. Um, C.Y. Wang, K.S. Chen, J. Electrochem. Soc. 147 (2000) 4485–4493.
[31] P. Costamagna, K. Honegger, J. Electrochem. Soc. 145 (1998) 3995–4007.
[32] J.M. Stockie, K. Promislow, B.R. Wetton, Int. J. Numer. Methods Fluids 41 (2003) 577–599.
[33] Elaine S. Oran, Jay P. Boris, Numerical Simulation of Reactive Flow, Cambridge University Press, 2001.
[34] Gyung Jin Park, Analytic Methods for Design Practice, Springer, 2007.
[35] M. Venkatraman, S. Shimpalee, J.W. Van Zee, Sung In Moon, C.W. Extrand, Int. J. Hydrogen Energy 34 (2009) 5522–5528.